

A Hybrid of Interval Wavelets and Wavelet Finite Element Model for Damage Detection in Structures

Jiawei Xiang¹, Toshiro Matsumoto², Yanxue Wang³ and Zhansi Jiang⁴

Abstract: Damages occurred in a structure will lead to changes in modal parameters (natural frequencies and modal shapes). The relationship between modal parameters and damage parameters (locations and depths) is very complicated. Single detection method using natural frequencies or modal shapes can not obtain robust damage detection results from the inevitably noise-contaminated modal parameters. To eliminate the complexity, a hybrid approach using both of wavelets on the interval (interval wavelets) method and wavelet finite element model-based method is proposed to detect damage locations and depths. To avoid the boundary distortion phenomenon, Interval wavelets are employed to analyze the finite-length modal shape to decompose into approximation and detailed signals. Damage locations will be detected by showing some peaks on the figures of detailed signal. To detect damage depths, the relationship between natural frequencies and damage depths (the damage depth detection database) is constructed using wavelet finite element method. Several natural frequencies obtained by experimental modal analysis are employed as inputs to the constructed database using particle swarm optimization (PSO) to search for damage depths. Numerical examples of beam and plate structures show that the new approach is robust to boundary distortion phenomenon and environment noise.

Keywords: Beam and plate, interval wavelets, wavelet Finite element model, Hybrid approach, Particle swarm optimization, Damage detection, Boundary dis-

¹ Department of Mechanical Science and Engineering, Nagoya University, Furo-cho, Chikusa-ku, Nagoya, 464-8603, Japan; School of Mechanical and Electrical Engineering, Guilin University of Electronic Technology, Guilin, 541004, China. Corresponding Author: Jiawei Xiang, E-mail: wxw8627@163.com

² Department of Mechanical Science and Engineering, Nagoya University, Furo-cho, Chikusa-ku, Nagoya, 464-8603, Japan

³ School of Mechanical and Electrical Engineering, Guilin University of Electronic Technology, Guilin, 541004, China

⁴ School of Mechanical and Electrical Engineering, Guilin University of Electronic Technology, Guilin, 541004, China

tortion phenomenon

1 Introduction

Due to the damage accumulation of aging structures in many civil and mechanical systems, the ability to monitor the structural health of these systems is becoming increasingly important. Several highly effective local non-destructive evaluation approaches (Qu and Li, 2010) are available. Vibration-based damage detection methods such as those due to the change of modal parameters (natural frequencies and modal shapes), have been utilized for identifying surface damages in structures (Ye et al., 2010; Xiang and Liang, 2011). The main advantage of vibration-based methods is that they have the ability to monitor damage locations and depths in the structure on a global basis. Modal shapes (Gökdağ and Kopmaz, 2009; rabowska et al., 2010; Cao et al., 2011) and natural frequencies (Murigendrappa et al., 2004; Patil and Maiti, 2003; Patil and Maiti, 2005; Maiti and Patil, 2005) are widely used to detect damage locations and depths. However, these monitoring methods used only one step (single detection method) to detect damage parameters (damage locations and depths) from the changes of natural frequencies or modal shapes of the damaged structures.

Generally, the relationship between natural frequencies (or modal shapes) and the corresponding damage parameters (damage locations and depths) is very complicated. Therefore, the single detection method using natural frequencies (or modal shapes) can not obtain robust damage detection results from the inevitably noise-contaminated modal parameters (Chen et al., 2005). As we known, the modal shape of damaged structures contains local singularity information, and can not be directly observed. The detection of singularities with wavelet transform has been studied not only in mathematics but also in signal processing (Mallat, 2008). Therefore, wavelet transform can also be employed to detect singular locations (damage locations) from modal shape. This method is made attractive by the availability of recent laser-technology (Siringoringo and Fujino, 2009) joined to accurate and fast scanning devices which allows to measure the modal shape of large and complex structures. However, wavelets are generally constructed on the whole real line and the discrete wavelet transform is defined for an infinite signal. In modal test, only finite points are obtained to generate modal shapes of a structure. When the wavelet transform is applied to decompose modal shape (finite signal), the so-called boundary distortion phenomenon (Strang and Nguyen, 1996; Mallat, 2008) will inevitably occur. This phenomenon would enormously influence the singularity detection results, especially for small data sets. To avoid boundary distortion phenomenon, several methods based on signal extension on the boundaries are presented, such as zero-padding, symmetrization and smooth padding, etc. (Strang and

Nguyen, 1996; Mallat, 2008). The other kind of method is wavelets on the interval (interval wavelets), which is an interesting construction both in theory (Cohen et al., 1993) and practical applications (Yan et al., 2008).

Generally, a reliable vibration-based damage detection system is divided into 4 levels: identification of damage that has occurred at very early stage (Level I), localization of damage (Level II), quantification of damage (Level III), and prediction of the remaining useful life of the structure (Level IV)(Worden et al., 2007). Focused on Level II and Level III, the purpose of this paper is to describe a robust hybrid approach for the detection of locations and depths of multiple damages in structures using wavelets on the interval (detect damage locations) and wavelet finite element model-based method (detect damage depths). With this method, the crack locations are first detected from a modal shape using interval wavelets and one of the detailed signals of modal shape will show some peaks at the corresponding damage locations. Interval wavelets can enormously eliminate boundary distortion of detailed signals. Further, to improve the detection precision, envelope detection is applied to the detailed signals and the multiple damage locations are displayed in the corresponding wavelet decomposition map. Then, the wavelet finite element method are employed to obtain damage detection databases of the multiple unknown damage depths for the known locations. The solution of inverse problem is essentially an optimization problem. Once the natural frequencies are measured from actual damaged structures, the computational intelligence techniques, such as support vector regression (SVR), genetic algorithm (GA), neural networks (NNs), particle swarm optimization (PSO), etc. (Marwala, 2010), can be employed as a useful tool to seek the damage depths from the available damage detection database.

The rest of the paper is organized as follows. The next section introduces a brief review of Daubechies interval wavelets. Section 3 introduces the hybrid approach using interval wavelet method and wavelet finite element model-based method to detect damage locations and depths, respectively. Numerical examples are presented in sections 4.

2 A brief review of Daubechies interval wavelets

Daubechies wavelets (Strang and Nguyen, 1996; Mallat, 2008) has proven to be a useful tool in the decomposition of signal. The support of the scaling function is

$$\text{supp}\phi_p = [0, 2p - 1], p \in Z^+ \quad (1)$$

where p denote the vanishing moment.

The wavelet function ψ has the p th vanishing moment, which is represented by

$$\int_{-\infty}^{+\infty} x^k \psi_p(x) dx = 0, k = 0, 1, \dots, p - 1 \tag{2}$$

Daubechies wavelets are classified according to the number of vanishing moments. For example, the three-order Daubechies wavelet, abbreviated Db3, indicate that the wavelet function has three vanishing moments.

The function or the signal f can be decomposed by wavelet function as

$$Proj_{V_{j+1}} f = \sum_k \langle f, \phi_{j+1,k} \rangle \phi_{j+1,k} = Proj_{V_j} f + \sum_k \langle f, \psi_{j,k} \rangle \psi_{j,k} \tag{3}$$

where $Proj_{V_{j+1}} f$ and $Proj_{V_j} f$ are the projections of signal f onto scaling space V_{j+1} and V_j , respectively. $\langle \cdot, \cdot \rangle$ denotes inner product, j and k are the scale and translation factors respectively.

The nesting and orthogonal properties cause the functions ϕ to be linked via two-scale relation

$$\phi(x) = \sum_{i=0}^{2N-1} p_i \phi(2x - i) \tag{4}$$

Once the filter coefficients p_i have been identified and ϕ has been constructed, the associated wavelet can be expressed by

$$\psi(x) = \sum_{i=2-2N}^1 (-1)^i p_{1-i} \phi(2x - i) \tag{5}$$

The scaling function and wavelet of Db3 are shown in Figs. 1(a) and (b) respectively.

To eliminate boundary distortion phenomenon, the construction of suitable interval wavelets has become a topic of interest. Interval wavelets are the construction of special boundary wavelets together with the usual wavelets for the interior within the interval to generate a multiresolution analysis (MRA) on the interval (Cohen et al., 1993).

Interval functions are used as collectives term for both the boundary and interior functions. The interval scaling and wavelet functions are given by

$$\begin{cases} \phi^{int} = \{ \phi^{left}, \phi, \phi^{right} \} \\ \psi^{int} = \{ \psi^{left}, \psi, \psi^{right} \} \end{cases} \tag{6}$$

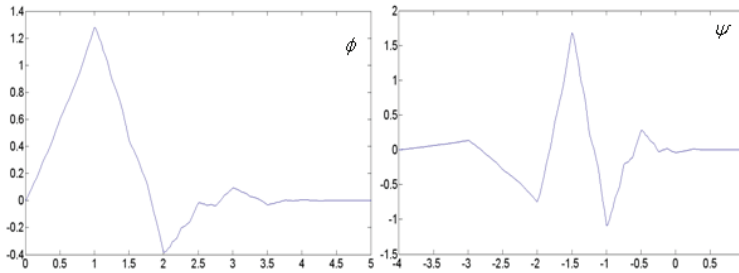


Figure 1: The scaling function and wavelet of Db3

where the superscripts of the boundary functions ϕ^{left} , ϕ^{right} , ψ^{left} and ψ^{right} denote the corresponding left and right interval boundaries.

Consider Daubechies basis with p vanishing moments and according to the Strang-Fix condition (Strang and Nguyen, 1996; Mallat, 2008), it appears that there exists a polynomial θ_k of degree k such that:

$$\sum_{n=-\infty}^{+\infty} n^k \phi(t-n) = \theta_k(t) \tag{7}$$

for $k < p$.

This equation is multiplied by $\chi_{[0,M]}(t)$, which is the indicator function of the interval $[0, M]$. Assuming that the support of ϕ is $[-p+1, p]$, scaling functions with indices $p \leq k < M-p$ are not changed by this restriction. To recover the Strang-Fix condition on the interval, p 'left' edge scaling function and p 'right' edge scaling functions are to be found such that

$$\begin{aligned} \theta_k(t)\chi_{[0,M]}(t) &= \sum_{n=-\infty}^{+\infty} n^k \phi(t-n)\chi_{[0,M]}(t) \\ &= \sum_{n=0}^{p-1} a[n]\phi_n^{left}(t) + \sum_{n=p}^{M-p-1} n^k \phi(t-n) + \sum_{n=0}^{p-1} b[n]\phi_n^{right}(t) \end{aligned} \tag{8}$$

If this equation is satisfied, it remains valid after rescaling. Therefore, we can find

the filters h and H which satisfy the scaling equation

$$\phi_{j,k}^{int} = \sum_{l=0}^{p-1} H_{k,l}^{left} \phi_{j+1,l}^{int} + \sum_{m=p}^{p+2k} h_{k,m}^{left} \phi_{j+1,m}^{int} \quad (9)$$

where $\phi_{j,k}^{int}$ denotes the whole set of scaling functions obtained by translation at the resolution j , and to verify the orthogonality condition. The coefficients of these filters are available in Ref. (Strang and Nguyen, 1996; Mallat, 2008).

In this paper, we use the source files of WAVELAB (Donoho et al., 2011) to write a program that detect damage locations in structures. Figs. 2 gives the boundary scaling functions and wavelets of Db3.

3 The hybrid approach to detect damage locations and depths

In the present investigation, we focus on the detection of q damages in structures. We use Daubechies interval wavelets to decompose on of the modal shapes so as to reveal the damaged locations. Then wavelet finite element method is employed to compute the damage detection database, i.e., the relationship between natural frequencies and damage depths. Damage depths can be detected using optimization method once several natural frequencies are obtained. It notes that in the present only numerical simulation is given to testify the proposed hybrid approach. The general steps for detecting damage locations and locations are listed below.

(1) Obtain modal shapes of damaged structures.

In the simulation, modal shapes of damaged structure is calculated using wavelet finite element method (Chen and Wu, 1995; Chen and Wu, 1996a, 1996b; Ma et al., 2003; Chen et al., 2004, 2006; Han et al., 2006, 2007, 2009; Xiang et al., 2009, 2010; Zhou and Zhou, 2008a, 2008b). Damages are modeled by the stiffness decreased at the damaged locations in structures. To show how the damages influence local stiffness in beam and plate structures, we make some explanation as fellows.

Figs. 3(a), (b) and (c) show the geometry, the cross-section and the model of a damaged beam, respectively. L is beam length, e_1, e_2, \dots, e_q denote the q damage locations, h is the height and b is the width of cross-section, c_1, c_2, \dots, c_q represent the q damage depths. The relative damage locations and depths are represented by $\beta_1 = e_1/L, \beta_2 = e_2/L, \dots, \beta_q = e_q/L$ and $\alpha_1 = c_1/h, \alpha_2 = c_2/h, \dots, \alpha_q = c_q/h$, respectively. The q damages can be represented by weightless rotational spring with stiffness expressed as $k_{r1}, k_{r2}, \dots, k_{rq}$ (Xiang et al., 2006, 2008a).

A plate with length l_x , width l_y and thickness t , is shown in Fig. 4 (a). Suppose q damages are occurred in the plate, the cross-section of damage i ($i = 1, 2, \dots, q$)

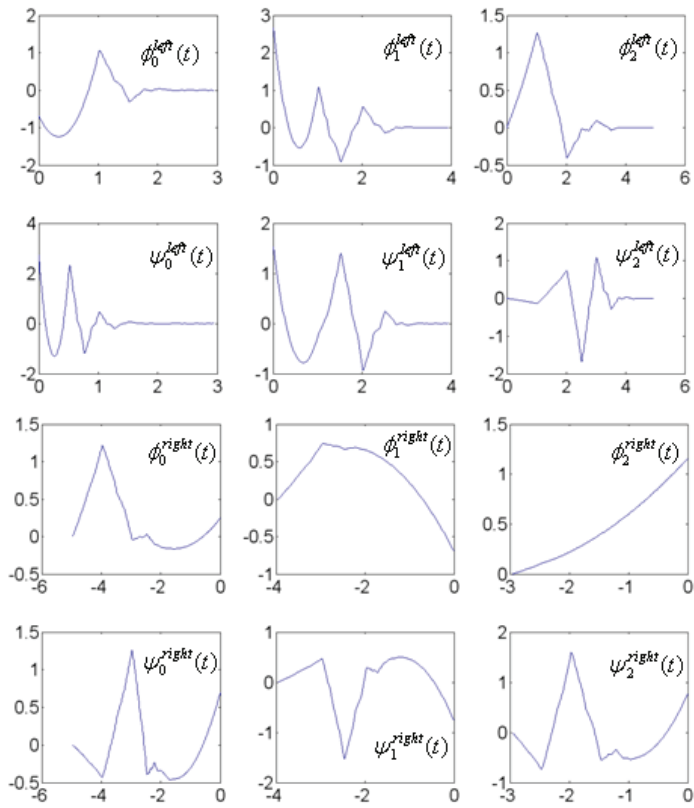


Figure 2: boundary scaling functions and wavelets with $p = 3$ vanishing moments

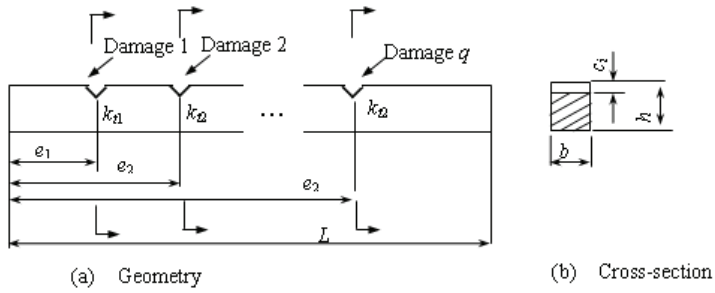


Figure 3: A beam with q open damages

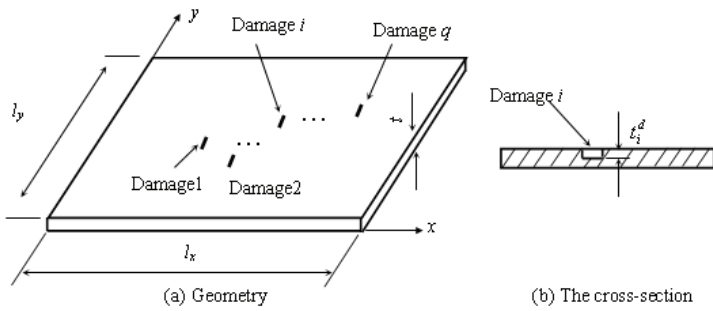


Figure 4: A plate with q damages

is shown in Fig.4(b) and the depth is $t_i^d (i = 1, 2, \dots, n)$. The stiffness matrix \mathbf{K} is proportional to t^3 (Xiang et al., 2008b). The q relative damage depths can be represented by

$$\alpha_i = \frac{t_i^d}{t} \quad (10)$$

Therefore, the corresponding row and column vectors in stiffness matrix \mathbf{K} will be multiplied by the reduction factor $\delta_i (i = 1, 2, \dots, k)$ on the corresponding damage areas. δ_i can be calculated as

$$\delta_i = (1 - \alpha_i)^3 \quad (11)$$

(2) Calculate wavelet coefficients for the selected modal shape use interval wavelets.

The approximation signal and several detailed signals are obtained by plotting the corresponding coefficients.

(3) Predict q damage locations from one of the detailed signals.

The peaks in the spatial distributions of the decomposed detailed signals denote the q damage locations. To reduce noise, the envelope technique (for one-dimensional structure) or soft threshold technique (for two-dimensional structure) are used in the present investigation.

(4) Construct wavelet finite element model to simulate damaged structures.

Once the wavelet finite element model of undamaged structures is built up, the reduction of the row and column vectors in the global stiffness matrix with respect to the damaged areas can be used to simulate damaged structure, whereas the global mass matrix remains unchanged.

(5) Calculate the natural frequencies with different damage depths for the known q damage locations.

The damage detection database can be obtained by the computation of different groups of damage depths $(\alpha_1, \alpha_2, \dots, \alpha_q)$ as

$$f_i = F_i(\alpha_1, \alpha_2, \dots, \alpha_q) \quad (12)$$

where F_i denote the discrete function relationship of the natural frequencies $f_i (i =$

$1, 2, \dots, n$) and the damage depths. It notes that $n \geq q$ is the necessary condition to obtain a stable solution of unknown $\alpha_i (i = 1, 2, \dots, q)$.

(6) Compute the noise-contaminated natural frequencies from simulation model by adding artificial noise.

(7) Use the intelligent optimization techniques to detect q damage depths from the constructed damage detection database.

In fact, the search of possible damage depths is essentially an optimization problem. Therefore, Support Vector Regression (SVR), Genetic Algorithm (GA), Neural Networks (NNs), Particle Swarm Optimization (PSO), etc., can be employed to seek the q depths.

4 Numerical simulation

In this section, two examples are given to verify the proposed approach. It notes that traditional Daubechies wavelet in associate with the classical boundary treatment method, e.g., zero-padding on the boundaries (Mallat, 2008), is employed.

Example 1 A cantilever beam with three damages

Suppose the beam dimensions and the material properties are: $L = 1m$, $b \times h = 0.02m \times 0.04m$, Young's modulus $E = 2.06 \times 10^{11} N/m^2$, material density $\rho = 7860 kg/m^3$, and Poisson's ratio $\mu = 0.3$. Damage case is considered as: $\beta_1 = 0.1$, $\beta_2 = 0.3$, $\beta_3 = 0.5$ and $\alpha_1 = 0.4$, $\alpha_2 = 0.5$, $\alpha_3 = 0.3$. BSWI (B-spline wavelets on the interval) wavelet finite element method has high precision by comparing with traditional finite element method, especially for the high gradient and crack singularity problems (Xiang et al., 2008a). Therefore, the wavelet-based numerical method is employed to simulate the modal parameters (natural frequencies and modal shapes) of damaged structure. in this example, damages can be represented by weightless rotational spring with stiffness expressed as $k_{t1}, k_{t2}, \dots, k_{tq}$ (Xiang et al., 2006). This representation is also the reduction of stiffness with respect to the damaged areas.

The third noise-free modal shape S and its wavelet decomposition (the decomposition level is 3) using Db3 wavelets and Db3 interval wavelets are shown in Figs.5 and 6, respectively. About half segment of the beam are decomposed by two kinds of wavelet decomposition. It notes that the modal shape S is calculated by 60 BSWI₄₃ (subscripts 4 and 3 denote the order and the level of BSWI) beam elements (Xiang et al., 2006) with 545 degrees of freedom (DOFs). The horizontal

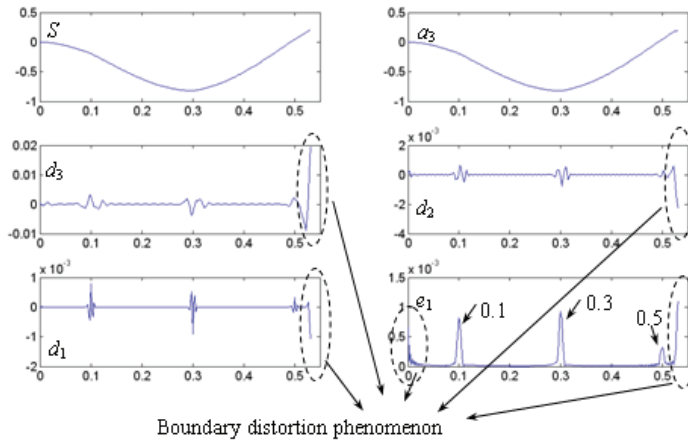


Figure 5: The 3th noise-free modal shape S_N and its wavelet decomposition using Db3 wavelets at level 3

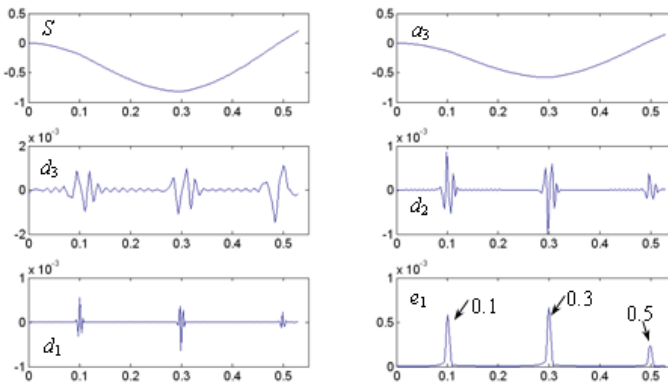


Figure 6: The 3th noise-free modal shape S_N and its wavelet decomposition using Db3 interval wavelets at level 3

coordinate of all subplots denote the relative location. Parameters d_1, d_2, d_3 and a_3 are respectively the detailed signals at three decomposition levels and the approximation signal, e_1 represents the envelope signal of d_1 . From Fig. 6, the crack locations can be seen vaguely in d_1, d_2, d_3 but more clearly in e_1 . The peak points are the predicted crack locations, i.e., $\beta_1^* = 0.1, \beta_2^* = 0.3, \beta_3^* = 0.5$ and the predictions for the three damage locations are 100 % accurate. Therefore, the locations of the three cracks can be detected accurately by looking at singular points from one of the detail signal decomposed from the modal shape. From Fig.5, we can see clearly that the boundary distortion phenomenon are occurred at both the edge of detailed signal d_1, d_2, d_3 and also the envelope signal e_1 . This phenomenon will significantly influence the detected damage locations which near the edge of structure. This investigation shows that wavelet on the interval has somewhat merits to deal with this problem.

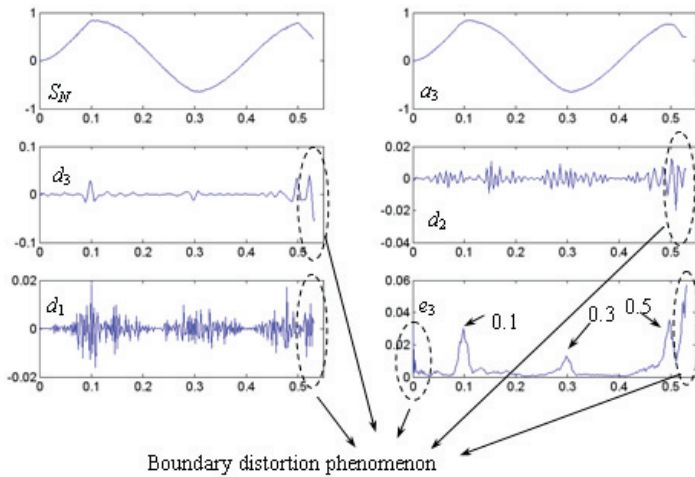


Figure 7: The 6th noise-contaminated modal shape S_N and its wavelet decomposition using Db3 wavelets at level 3

The sixth noise-contaminated modal shape S_N ($\pm 2\%$ artificial white Gaussian noise is added and calculated by $S_N = (1 + 2 \times (2 \times rand - 1) / 100) \times S$) is shown in Figs. 7 and 8. The horizontal coordinate of each subplot denotes the relative location and also about half segment of the beam is considered. We also use Db3 wavelets and Db3 interval wavelets to decompose the signal S_N . Parameters d_1, d_2, d_3 and a_3 are

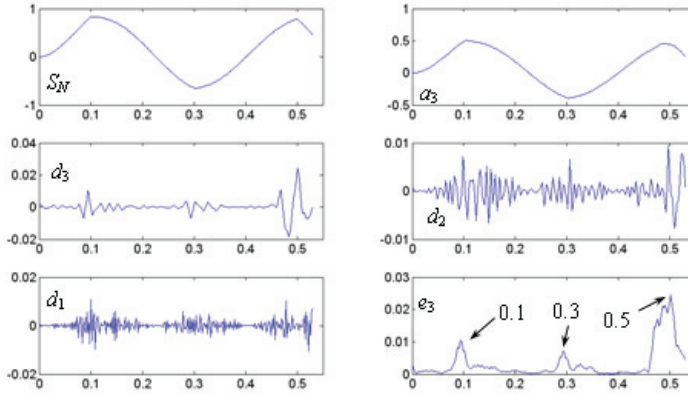


Figure 8: The 6th noise-contaminated modal shape S_N and its wavelet decomposition using Db3 interval wavelets at level 3

respectively the detailed signals at three decomposition levels and the approximation signal, e_3 represents the envelope signal of d_3 . The peak points in subplot e_3 from Fig. 8, are the predicted damage locations $\beta_1^* = 0.1$, $\beta_2^* = 0.3$, $\beta_3^* = 0.5$. The predications for the three cases are 100 % accurate. However, the locations of the third damage can not be distinguished from the peak caused by boundary distortion in subplot e_3 from Fig.7. Therefore, we can not judge whether it surely exists a damage at $\beta_3^* = 0.5$ or not.

Based on the above investigation, we can conclude that the boundary distortion phenomenon is enormously eliminated using interval wavelets and the advantage of interval wavelets is also testified. For a finite date point, Daubechies wavelets can not effectively eliminate the boundary distortion phenomenon. This will lead the aliasing when the damage is occurred at the edge of a structure.

The damage depths can not be determined from the information of the singular points. Therefore, we need another technique to estimate damage depths, as described clearly in section 3 (steps (4)~(7)). To obtain the damage detection database, we calculate the natural frequencies with different damage depths for the three detected damage locations.

When damage locations $\beta_1 = 0.1$, $\beta_2 = 0.3$ and $\beta_3 = 0.5$ are detected, the six natural frequencies for a definitely damage depths $\alpha_1 = 0.4$, $\alpha_2 = 0.5$ and $\alpha_3 = 0.3$, are computed by 10 BSWI₄₃ beam elements, i.e., $f_1 = 27.76Hz$, $f_2 = 188.09Hz$,

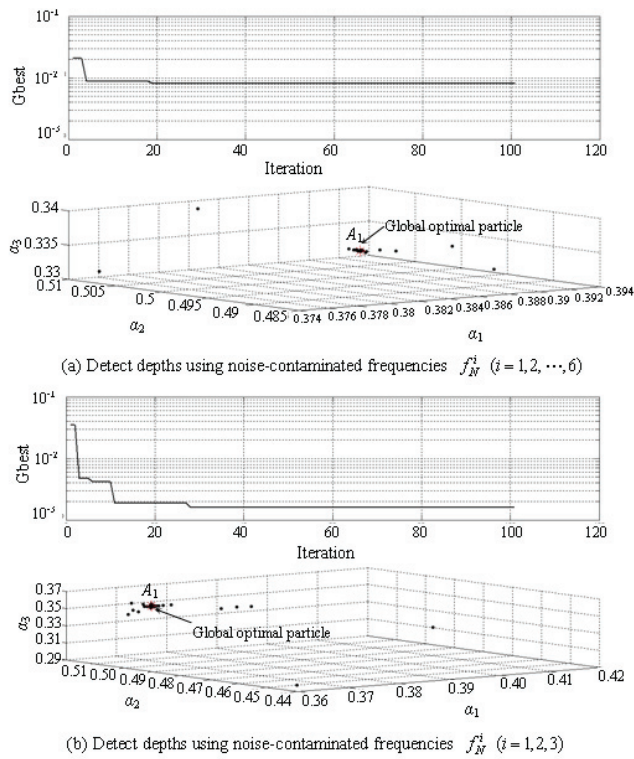


Figure 9: The PSO convergence progress and the optimal particle location

$f_3 = 526.62Hz$, $f_4 = 1064.33Hz$, $f_5 = 1836.02Hz$ and $f_6 = 2465.79Hz$, respectively. We add $\pm 1\%$ noise to the six natural frequencies (calculated by $f_N^i = (1 + 1 \times (2 \times rand - 1)/100) \times f_i$) to simulate frequency measurement errors and the noise-contaminated natural frequencies are: $f_N^1 = 27.94Hz$, $f_N^2 = 186.35Hz$, $f_N^3 = 525.25Hz$, $f_N^4 = 1060.61Hz$, $f_N^5 = 1843.89Hz$ and $f_N^6 = 2455.34Hz$.

In the simulation, we use PSO to search for the three depths from the available damage detection database F_i as shown in Eq. (12). we use the following objective or fitness function to search for the "best fit" damage depths as

$$\min \sum_{i=1}^n \left\| \frac{f_i - f_N^i}{f_i} \right\|_2 \tag{13}$$

$$s.t. \quad 0.1 < \alpha_j < 0.9, \quad j = 1, 2, \dots, q \tag{14}$$

where $\| \cdot \|_2$ is the Euclidean norm, constraint limits the damage depth search space from 0.1 to 0.9, f_N^i is the "measured" natural frequencies (for the simulation purpose, only the calculated noise-contaminated natural frequencies are employed).

In this example, to obtain a more accurate damage depths detection database, α_1 , α_2 and α_3 are varied from 0.1 to 0.9 with step length of 0.01. Therefore, there are 531441 ($= 81 \times 81 \times 81$) data points in the search space of the discrete functions $F_i (i = 1, 2, \dots, n)$. The optimization is implemented with MATLAB using a PSO Toolbox coded by Birge (Birge, 2003). More information about the Toolbox can be found in its help documents. In this investigation, a population of 50 individuals is used as particles. According to the recommendations by Birge, the values of the cognition learning and the social learning factors c_1 and c_2 are both set to 2, the maximum particle fly speed is fixed at 10 % of the range of α_1 , α_2 and α_3 . The value of inertia weight w decreases linearly from 0.9 in the first iteration to 0.4 for the 100th iteration. The convergence is reached long before 100 iterations. Because the PSO is for continuous variable optimization problems, the α_1 , α_2 and α_3 values provided by the PSO algorithm may not be discrete. Therefore, the α_1 , α_2 and α_3 outputs in each iteration should be rounded up and down to the nearest discrete numbers.

Fig.9 (a) and (b) shows the search convergence process and the global optimization particle locations for the usage of six ($f_N^1, f_N^2, f_N^3, f_N^4, f_N^5, f_N^6$) and three (f_N^1, f_N^2, f_N^3) noise-contaminated natural frequencies, respectively. The damage detection results revealed by the coordinate values of A_1 , as show in Fig.9 (a) and (b), are: $\alpha_1^* = 0.39$, $\alpha_2^* = 0.5$ and $\alpha_3^* = 0.33$ for six natural frequencies case and $\alpha_1^* = 0.37$, $\alpha_2^* = 0.51$ and $\alpha_3^* = 0.35$ for three natural frequencies case, respectively. From the comparison, we can see clearly that the number of natural frequencies affects detection results. The PSO algorithms achieve the best solutions in less than 20

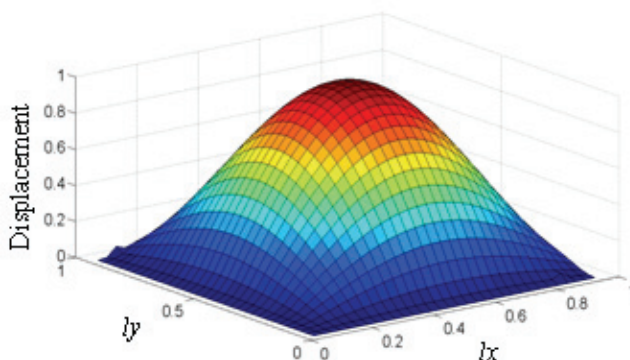


Figure 10: The first modal shape of simply supported plate with two damages

iterations for the six natural frequencies case, whereas it attain to 27 iterations (a little extra interactions are need) for the three natural frequencies case, as shown in the upper figures in Fig.9 (a) and (b) respectively. Therefore, it is seemly preferred to use as many natural frequencies as possible to improve detection accuracy. In order to make a relatively complete comparison, additional fifteen different damage depth combinations as specified by different α_1, α_2 and α_3 , are represented by Case 1 to Case 15, as shown in Table 1. The noise-free natural frequencies $f_i (i = 1, \dots, 6)$ and the noise-contaminated $f_N^i (i = 1, \dots, 6)$ are shown in Tables 1 and 2, respectively. We compared the detection results using two combinations of noise-contaminated frequencies, i.e., (f_N^1, f_N^2, f_N^3) , and $(f_N^1, f_N^2, f_N^3, f_N^4, f_N^5, f_N^6)$ for the fifteen cases, respectively. The results are summarized in Tables 3. As shown in the table, with (f_N^1, f_N^2, f_N^3) , the detection errors for depths of damages 1, 2 and 3 are in the range of 0% to 7% with means of 2.47%, 2.2% and 3%, respectively. When combination $(f_N^1, f_N^2, f_N^3, f_N^4, f_N^5, f_N^6)$ is used, the errors vary from 0% to 7% and the mean errors reduce to 1.93%, 1.67% and 1.73% for the three damages. These results seem to suggest that the use of high natural frequencies yields a little better detection results.

The above results demonstrate that the PSO algorithm is effective in detecting damage depths and it yields reasonably good results when the data contain certain level of noise.

Table 1: The first six noise-free natural frequencies for different damage case

Case	Damage depth			Noise-free natural frequencies (Hz)					
	α_1	α_2	α_3	f_1	f_2	f_3	f_4	f_5	f_6
1	0.1	0.2	0.2	32.38	202.82	572.22	1113.74	1875.87	2722.82
2	0.2	0.3	0.3	31.25	196.65	561.67	1085.21	1867.95	2623.31
3	0.2	0.3	0.1	31.47	203.03	561.87	1120.42	1867.98	2692.66
4	0.3	0.3	0.1	30.58	200.81	560.6	1120.36	1861.18	2668.56
5	0.4	0.3	0.1	29.27	197.81	558.91	1120.29	1851.62	2635.86
6	0.3	0.4	0.1	29.87	197.05	546.67	1097.76	1855.04	2586.88
7	0.3	0.4	0.3	29.75	193.22	546.37	1075.49	1854.96	2549.37
8	0.3	0.4	0.4	29.55	187.52	545.91	1045.21	1854.85	2501.8
9	0.5	0.5	0.1	26.42	189.59	525.17	1101.55	1822.64	2486.26
10	0.5	0.5	0.2	26.38	187.51	524.76	1087.24	1822.42	2466.23
11	0.5	0.5	0.3	26.29	183.96	524.06	1064.33	1822.08	2435.52
12	0.4	0.6	0.2	26.84	188.98	508.38	1076.79	1827.13	2444.72
13	0.4	0.6	0.3	26.75	185.7	507.25	1053.26	1826.83	2415.08
14	0.4	0.6	0.4	26.61	180.76	505.57	1021.32	1826.42	2377.4
15	0.3	0.7	0.5	26.1	176.36	486.26	973.02	1830.58	2322.07

Example 2 A simply supported plate with two damages

A simply supported structure with length $lx = 1m$, width $ly = 1m$ and thickness $t = 0.01m$, as shown in Fig. 4 (a). Suppose two small damages are occurred on the surface of structure, the cross-section of damage i ($i = 1, 2$) is shown in Fig.4(b) and the depth is t_i^d ($i = 1, 2$). Material parameters are: Young’s modulus $E = 206GPa$, Possion’s ratio $\mu = 0.3$ and material density $\rho = 7860Kg/m^3$.

Suppose two damages are occurred at two locations ($x_1 = 0.059m, y_1 = 0.912m$ and $x_2 = 0.824m, y_2 = 0.029m$) and the corresponding severities are both represented by the reduction of the $t = 0.01m$ to $t_1^d=t_2^d=0.0013m$. The two damage depth $\alpha_1 = \alpha_2 = 0.13$.

BSWI₄₅ (subscripts 4 and 5 denote the order and the level of BSWI) scaling functions (Xiang et al., 2007) are employed as approximation bases to calculate this problem. The corresponding row and column in stiffness matrix \mathbf{K} will be multiplied by the factors $\delta_1 = \delta_2 = 0.659$ in the corresponding damage locations.

The first modal shape shown in Fig.10 is available on a 35×35 sample grid. For

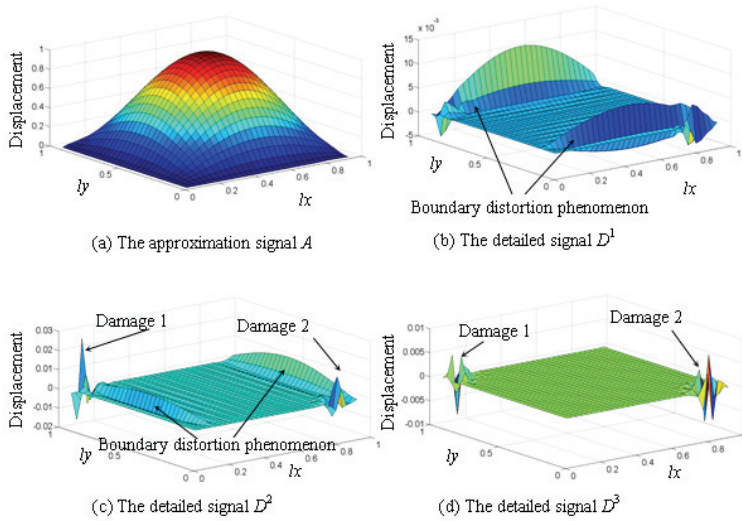


Figure 11: The decomposition results of the first modal shape using Db3 wavelets

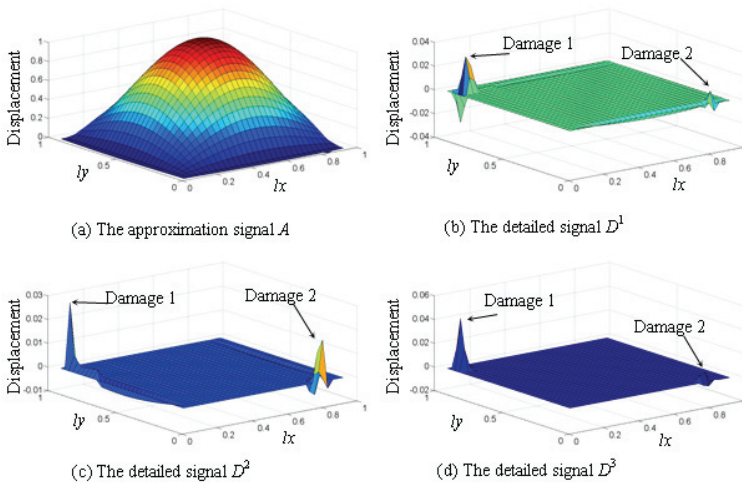


Figure 12: The decomposition results of the first modal shape using Db3 interval wavelets

Table 2: The first six noise-contaminated natural frequencies for different damage cases

Case	Noise-contaminated natural frequencies(1% noise, Hz)					
	f_N^1	f_N^2	f_N^3	f_N^4	f_N^5	f_N^6
1	32.11	201.01	572.57	1119.96	1892.15	2702.67
2	31.29	196.53	556.19	1081.68	1855.33	2638.75
3	31.35	203.14	558.11	1122.7	1859.12	2700.96
4	30.69	201.81	560.04	1111.04	1851.09	2690.62
5	29.07	199.1	559.34	1131.41	1836	2632.83
6	29.64	198.87	541.26	1103.79	1866.81	2605.96
7	29.9	192.2	542.4	1068.76	1848.14	2565.34
8	29.51	186.75	541.17	1049.35	1850.38	2525.43
9	26.62	189	526.85	1092.12	1813.96	2502.42
10	26.54	185.94	528.64	1076.39	1809.8	2478.89
11	26.25	182.3	528.28	1073.8	1821.75	2435
12	26.84	190.81	505.23	1078.59	1839.49	2447.81
13	26.61	187.05	504.58	1049.83	1827.74	2438.59
14	26.65	179.17	502.89	1018.32	1838.15	2354.36
15	25.86	175.19	487.71	977.53	1835.99	2319.79

the analysis, 2-D Db3 is used to decompose at one level. Fig.11 shows the decomposition results of the first modal shape using Db3 wavelets. The approximation signal A as shown in Fig. 11(a) is essentially a smoothed version of the first modal shape where high frequencies have been removed. The horizontal detailed signal D^1 , the vertical detail D^2 and diagonal detail D^3 are shown in Fig. 11 (b), (c) and (d), respectively. As shown in these figures, D^1 , D^2 and D^3 are all sensitive to damage singularity. However, the horizontal detailed signal D^1 , the vertical detailed signal D^2 and diagonal detail D^3 also show the severe boundary distortions that usually occur in wavelet coefficient computation near the signal edges (it means plate edges). This phenomenon will significantly influence the detected damage locations which near the edge of structure.

Fig.12 shows the decomposition results of the first modal shape using Db3 interval wavelets. The two peaks reveal the damage singularity and the locations of show in Fig.12 (b), (c) and (d) clearly indicate the two predicted damage locations, i.e., $(x_1^* = 0.059m, y_1^* = 0.912m)$ and $(x_2^* = 0.824m, y_2^* = 0.029m)$. Compared with the Daubechies wavelet decomposition, interval wavelets decomposition will enor-

Table 3: The damage detection results using three and six noise-contaminated frequencies (ε is the detection error, $\varepsilon_i = |\alpha_i^* - \alpha_i| \times 100\%$)

Case	Detection results using $f_N^i (i = 1, 2, 3)$						Detection results using $f_N^i (i = 1, \dots, 6)$					
	α_1^*	α_2^*	α_3^*	$\varepsilon_1(\%)$	$\varepsilon_2(\%)$	$\varepsilon_3(\%)$	α_1^*	α_2^*	α_3^*	$\varepsilon_1(\%)$	$\varepsilon_2(\%)$	$\varepsilon_3(\%)$
1	0.16	0.19	0.23	6	1	3	0.17	0.19	0.21	7	1	1
2	0.14	0.35	0.31	6	5	1	0.17	0.33	0.29	3	3	1
3	0.19	0.33	0.10	1	3	0	0.20	0.31	0.10	0	1	0
4	0.28	0.31	0.10	2	1	0	0.28	0.30	0.11	2	0	1
5	0.41	0.29	0.10	1	1	0	0.41	0.29	0.10	1	1	0
6	0.30	0.44	0.10	0	4	0	0.30	0.43	0.10	0	3	0
7	0.25	0.43	0.34	5	3	4	0.28	0.41	0.31	2	1	1
8	0.27	0.43	0.42	3	3	2	0.30	0.41	0.39	0	1	1
9	0.49	0.49	0.17	1	1	7	0.49	0.49	0.16	1	1	6
10	0.50	0.47	0.27	0	3	7	0.50	0.47	0.26	0	3	6
11	0.51	0.48	0.34	1	2	4	0.52	0.47	0.31	2	3	1
12	0.38	0.62	0.13	2	2	7	0.36	0.63	0.17	4	3	3
13	0.40	0.62	0.25	0	2	5	0.39	0.62	0.28	1	2	2
14	0.38	0.61	0.44	2	1	4	0.39	0.61	0.42	1	1	2
15	0.35	0.69	0.49	5	1	1	0.35	0.69	0.49	5	1	1
Average errors				2.47	2.2	3				1.93	1.67	1.73

mously decreased boundary distortion phenomenon for the detailed signals D^1 , D^2 and D^3 . The predications for the two damage locations are 100 % accurate. Therefore, the advantage of interval wavelets is also testified by two-dimensional damage detection problem. For the finite date point, Daubechies wavelet can not effectively eliminate the boundary distortion phenomenon. Therefore, it will lead to the wrong detection results when damages are occurred at the edge of structure.

The proposed approach is also tested for its noise robustness by adding $\pm 2\%$ level of artificial white Gaussian noise to the first modal shape, i.e., $S_N = (1 + 2 \times (2 \times rand - 1) / 100 \times S)$, where S_N is the noise-contaminated modal shape, S is the noise-free modal shape. The approximation signal A and the detailed signals D^1 , D^2 and D^3 of the noise-contaminated modal shape using Db3 wavelets and Db3 interval wavelets, are displayed in Fig. 13 and Fig. 14, respectively. The influence of the noise is noticeable in all detailed signals. This implies that for a small damage, the singularities caused by the damage may be masked by the noise-caused

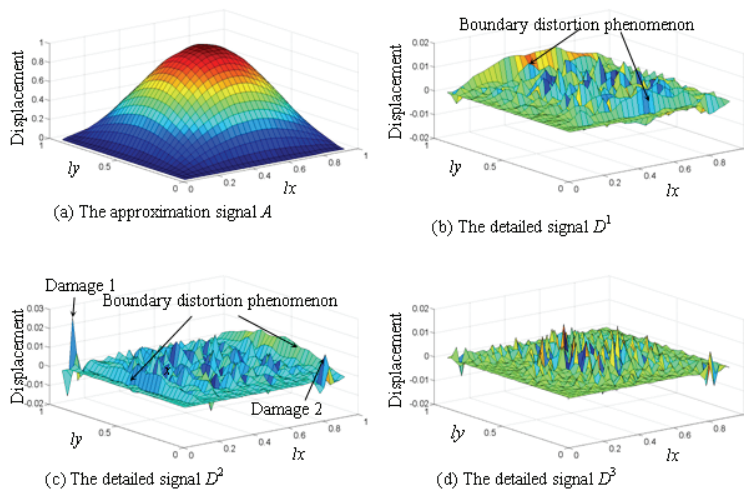


Figure 13: The decomposition results of the modal shape obtained from noisy data using Db3 wavelets

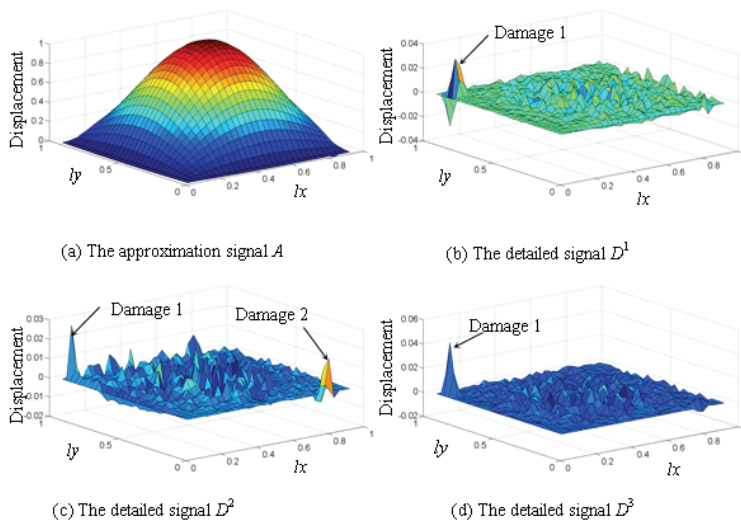


Figure 14: The decomposition results of the modal shape obtained from noisy data using Db3 interval wavelets

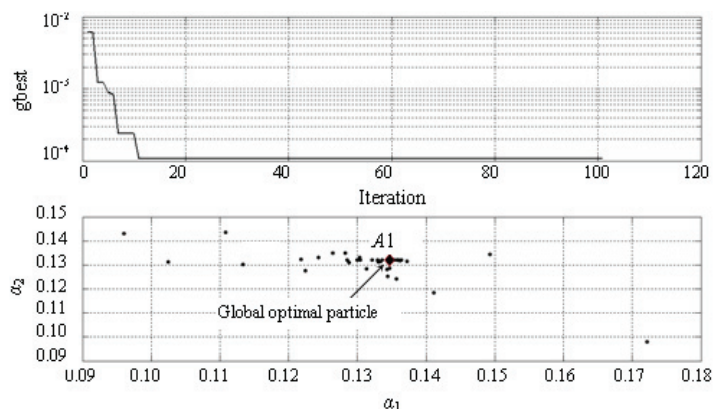


Figure 15: The PSO convergence progress and the optimal particle location (damage depths) using noise-contaminated frequencies $f_N^i (i = 1, 2)$

peaks. Compared D^1 , D^2 and D^3 in Fig.13 (b), (c) and (d) with those in Fig.14 (b), (c) and (d), we can see clearly that the decomposition results using Db3 interval wavelets is better than those using Db3 wavelets. For the dual impacts of noise and boundary distortion phenomenon, it is difficult to reveal the damages from the noise and the boundary distortion induced peaks. From Fig. 13(c), the coordinate of two predicted damage locations can not be uniquely determined, whereas in Fig. 14(c), the two predicted damage locations, i.e., $(x_1^* = 0.059m, y_1^* = 0.912m)$ and $(x_2^* = 0.824m, y_2^* = 0.029m)$, are uniquely determined with 100 % accurate.

From the above analysis, the method proposed in this paper is relatively simple as only a single scale decomposition of the first modal shape of structure is sufficient.

The PSO is also employed to detect the two damage depths. As mentioned in Section 3, $n \geq q$ is the necessary condition to obtain a robust solution of unknown damage depth q . Therefore, we use two noise-contaminated natural frequencies f_N^1 and f_N^2 to detect damage depth α_1 and α_2 . The BSWI₄₅ scaling functions (Xiang et al., 2007) are employed to calculate the damage detection database. To obtain a more accurate severity evaluation database, α_1 and α_2 are varied from 0.1 to 0.9 with step length of 0.01. Therefore, there are 6561 ($= 81 \times 81$) data points in the search space of the discrete functions $f_i = F_i(\alpha_1, \alpha_2)$. For the given damage depths $\alpha_1 = \alpha_2 = 0.13$, the noise-free natural frequencies $f_1 = 48.68Hz$ and $f_2 = 121.62Hz$. Suppose $\lambda\%$ noise is added to the noise-free frequencies according to

$f_N^i = (1 + 1 \times (2 \times rand - 1)/100) \times f_i$, $i = 1, 2$, we have the noise-contaminated frequencies $f_N^1 = 49.12Hz$ and $f_N^2 = 122.18Hz$. The PSO parameters are given similarly to those in Example 1. The search convergence process and the global optimization particle locations for $f_N^1 = 49.12Hz$ and $f_N^2 = 122.18Hz$ are shown in Fig. 15. The PSO algorithms achieve the best solutions in less than 15 iterations whereas the global optimization particles are located at point A_1 , i.e., the predicted damage depths are $\alpha_1^* = 0.134$ and $\alpha_2^* = 0.131$. The small detection errors indicate that the PSO algorithm yields reasonably good results when the data contain certain level of noise.

5 Conclusion

This paper suggests a hybrid methodology based on interval wavelet and wavelet finite element model to detect damage locations and depths in structures. The effectiveness of the proposed approach has been examined by numerical simulation of beam and plate structure. Damage location detection results show that the traditional boundary treatment method, e.g., zero-padding on the boundaries, can not effectively eliminate the boundary distortion phenomenon, whereas interval wavelet can eliminate this phenomenon occurred at the edges of beam and plate structures. PSO is also a good choice to detect damage depths to search for the damage depths from the damage detection database calculated by finite element method. It is believed that this hybrid approach can be easily extended to complex structures if one of the modal shapes and several natural frequencies of those structures are measured by scanning laser vibrometer.

Acknowledgement: The authors are grateful to the support of the Japan Society for the Promotion of Science (ID: P11052), the National Science Foundation of China (Nos. 51175097, 51165003, 51105085), GuangXi key Technologies R&D Program of China (Nos. 1099022-1, 10123005-12). This material is also based upon work funded by Zhejiang Technologies R&D Program of China (No. 2010C31094) and Zhejiang Provincial Natural Science Foundation of China under Grant No. Y1110046.

References

- Birge, B.**(2003): PSOT-a particle swarm optimization toolbox for use with Matlab. *Proceedings of the IEEE Swarm Intelligence Symposium (SIS03)*, Indianapolis, USA, pp. 182-186.
- Cao, M.S.; Ye, L.; Zhou, L.M.; Su, Z.Q.; Bai, R.B.**(2011):Sensitivity of fundamental mode shape and static deflection for damage identification in cantilever

beams. *Mechanical Systems and Signal Processing*, vol.25, pp.630-643.

Chen, W.H.; Wu, C.W.(1995): A spline wavelets element method for frame structures vibration. *Computational Mechanics*, vol.16, pp.11-21.

Chen, W.H.; Wu, C.W. (1996a): Extension of spline wavelets element method to membrane vibration analysis. *Computational Mechanics*, vol. 18, pp.46-54.

Chen, W.H.; Wu, C.W.(1996b): Adaptable Spline Element for Membrane Vibration Analysis. *International Journal for Numerical Methods in Engineering*, vol. 39,pp. 2457-2476.

Chen, X.F.; Yang S.J.; Ma, J.X.; He, Z.J.(2004): The construction of wavelet finite element and its application. *Finite Elements Analysis and Design*, vol.40, pp. 541-554.

Chen, X.F.; He, Z.J.; Li, B.(2005): An efficient wavelet finite element method in fault prognosis of incipient crack. *Science in China Series E: Technological Sciences*, vol.49, pp.89-101.

Chen ,X.F.; Zi, Y.Y.; Li, B.; He, Z.J.(2006): Identification of multiple cracks using a dynamic mesh-refinement method. *The Journal of Strain Analysis for Engineering Design*, vol. 41 , pp. 31-39.

Cohen, A.; Daubechies, I.; Vial, P.(1993): Wavelets on the interval and fast wavelet transform. *Applied and Computational Harmonic Analysis*, vol. 1, pp.54-81.

Donoho, D.; Maleki, A.; Shahram, M. (2011) <http://stat.stanford.edu/~wavelab/>.

Gökdağ, H. and Kopmaz, O.(2009):A new damage detection approach for beam-type structures based on the combination of continuous and discrete wavelet transforms. *Journal of Sound and Vibration*, vol.324, pp.1158-1180.

Han, J.G.; Ren, W.X.; Huang Y.(2006): A spline wavelet finite-element method in structural mechanics. *International Journal for Numerical Methods in Engineering*, vol.66, pp.166-190.

Han, J.G.; Ren, W.X.; Huang Y.(2007): A wavelet-based stochastic finite element method of thin plate bending. *Applied Mathematical Modelling*, vol.31, pp. 181-193.

Han, J.G.; Ren, W.X.; Huang Y.(2009): A spline wavelet finite element formulation of thin plate bending. *Engineering with Computers*, vol. 25, pp. 319-326.

Ma, J.X.; Xue, J.J.; Yang S.J.; He, Z.J.(2003): A study of the construction and application of a Daubechies wavelet-based beam element. *Finite Elements Analysis and Design* , vol. 39, pp.965-975.

Mallat, S.: *A Wavelet Tour of Signal Processing, 3rd ed.*. Academic Press, London,

2008.

Maiti S.K. and Patil, D.P. (2005): A method of analysis for detection of multiple cracks in beams based on vibration. *Advances in Vibration Engineering*, vol.3, pp.348-369.

Marwala, T.: *Finite-element-model Updating Using Computational Intelligence Techniques*. Springer-Verlag, London, 2010.

Murigendrappa, S.M.; Maiti, S.K.; Srirangarajan, H.R. (2004): Frequency-based experimental and theoretical identification of multiple cracks in straight pipes filled with fluid. *NDT & E International*, vol.37, pp.431-438.

Patil, D.P. and Maiti, S.K.(2003): Detection of multiple cracks using frequency measurements. *Engineering Fracture Mechanics*, vol.70, pp.1553-1572.

Patil, D.P. and Maiti, S.K.(2005): Experimental verification of a method of detection of multiple cracks in beams based on frequency measurements. *Journal of Sound and Vibration*, vol.281, pp.439-451.

Qu, J.P. and Li, H.(2010): Structural health monitoring in mainland China: review and future Trends. *Structural Health Monitoring*, vol.9, pp. 219-231.

rabowska, J.; Palacz, M.; Krawczuk, M.(2010):Damage identification by wavelet analysis. *Mechanical Systems and Signal Processing*, vol.22, pp.1625-1635.

Siringoringo, D.M.; Fujino, Y. (2009): Noncontact operational modal analysis of structural members by Laser Doppler Vibrometer. *Computer-Aided Civil and Infrastructure Engineering*, vol. 24, pp.249-265.

Strang, G. and Nguyen, T. : *Wavelets and filter banks*. Wellesley-Cambridge Press, London, 1996.

Worden, K.; Farrar, C.R.; Manson, G.; Park, G.(2007): The fundamental axioms of structural health monitoring. *Proceedings of the Royal Society of London, Series A*, vol. 463, pp. 1639-1664.

Xiang, J.W.; Chen,X. F.; He Y. M.; He,Z.J.(2006): Identification of crack in a beam based on finite element method of B-spline wavelet on the interval. *Journal of Sound and Vibration*, vol. 296, pp. 1046-1052.

Xiang, J.W.; Chen, X.F.; He, Z.J.; Dong, H.B.(2007): The construction of 1D wavelet finite elements for structural analysis. *Computational Mechanics*, vol.40, pp.325-339.

Xiang ,J.W.; Zhong,Y. T.; Chen,X.F.; He,Z.J.(2008a): Crack Detection in a Shaft by Combination of the New Wavelet-based Elements and Genetic Algorithm. *International Journal of Solids and Structures*, vol. 45, pp. 4782-4795.

Xiang, J.W., Chen, X.F., Yang L.F. and He, Z.J.(2008b): A Class of Wavelet-

based Flat Elements Using B-spline Wavelet on the Interval and Its applications. *CMES: Computer Modeling in Engineering and Sciences*, vol.23, pp.1-12.

Xiang, J.W.; Chen, D.D.; Chen, X.F.; He, Z.J.(2009): A novel wavelet-based finite element method for the analysis of rotor-bearing systems. *Finite Elements in Analysis and Design*, vol.45, pp.908-916.

Xiang, J.W.; Long, J.Q.; Jiang, Z.S.(2010): A numerical study using Hermite cubic spline wavelets for the analysis of shafts. *Proceedings of the Institution of Mechanical Engineers, Part C, Journal of Mechanical Engineering Science*, vol.224, pp.1843-1851.

Xiang, J.W. and Liang, M.(2011): Multiple damage detection method for beams based on multi-scale elements using Hermite cubic spline wavelet. *CMES: Computer Modeling in Engineering and Sciences*, vol.73, pp.1-32.

Yan, Z.Z.; Wang, Y.S.; Zhang C.Z.(2008): A method based on wavelets for band structure analysis of phononic crystals. *CMES: Computer Modeling in Engineering and Sciences*, vol. 38, pp.59-88.

Ye, J.J.; He, Y.M.; Chen, X.F.; He, Z.J.(2010):Pipe crack identification based on finite element method of second generation wavelets. *Mechanical Systems and Signal Processing*, vol.24, pp.379-393.

Zhou Y.H., Zhou J.(2008a): A modified wavelet approximation of deflections for solving PDEs of beams and square thin plates. *Finite Elements in Analysis and Design*, vol. 44, 773-783.

Zhou Y.H., Zhou J.(2008b): A modified wavelet approximation for multi-resolution AWCM in simulating nonlinear vibration of MDOF systems. *Computer Methods in Applied Mechanics and Engineering*, vol.197, pp.1466-1478.